International Communications in Heat and Mass Transfer 139 (2022) 106421

Contents lists available at ScienceDirect

International Communications in Heat and Mass Transfer

journal homepage: www.elsevier.com/locate/ichmt

Analysis of applying fin for charging process of phase change material inside H-shaped thermal storage

Mohsen Izadi [a,*], Ahmad Hajjar [b], Hashim M. Alshehri [c], Arslan Saleem [d], Ahmed M. Galal [e,f]

[a] Mechanical Engineering Department, Faculty of Engineering, Lorestan University, Khorramabad, Iran
[b] LabECAM, ECAM Lyon, Université de Lyon, Lyon, France
[c] Department of Mathematics, Faculty of Science, King Abdulaziz University, Jeddah 21521, Saudi Arabia
[d] School of Engineering, Cardiff University, Queen's Buildings, The Parade, CF24 3AA Cardiff, United Kingdom
[e] Mechanical Engineering Department, College of Engineering, Prince Sattam Bin Abdulaziz University, Wadi addawaser 11991, Saudi Arabia
[f] Production Engineering and Mechanical Design Department, Faculty of Engineering, Mansoura University, P.O 35516, Mansoura, Egypt

ARTICLE INFO

Keywords:
Finned thermal storage
Charging process
H-shaped
Fin angle

ABSTRACT

An H-shaped Double thermal storage unit has been studied numerically. A middle wall is sandwiched between two twin thermal storage cavities which are charging. The fins are attached to the middle wall to enhance the charging process. The set of equations modeling the charging process were solved using the Finite Element Method. The effects of different main parameters, namely thermal Fourier number, fin angle (symmetric cases) ($-60 \leq \lambda \leq 60$), 15 cases related to non-symmetric fin angle ($-60 \leq \lambda_l \leq 60$) and ($-60 \leq \lambda_r \leq 60$), and aspect ratio of fins (AR = 0.5–32) on the melting process of phase change material have been numerically studied. The results indicate that using fins for the cavity enhances the melting rate in the neighboring region due to the conductive heat transfer through the fins. Also, faster phase change material melting can be achieved by directing the fins upwards.

1. Introduction

To meet the world's ever-increasing energy demand, in the last decade, the focus has shifted towards harvesting renewable energy. Another problem gaining attention alongside harvesting energy is of storing that energy. Thermal energy storage operates on the simplistic approach of storing energy using some medium to be utilized later at any time. These are usually classified into three classes such as sensible heat storage, latent heat storage, and thermochemical heat storage, based on the operational methods. The sensible heat storage method depends on increasing the material temperature and storing the amount of energy based on the material's specific heat capacity. Whereas, thermochemical methods take advantage of the chemical reaction occurring between two chemical substances [1,2]. Latent heat storage methods rely on the heat released due to the phase transition of the materials commonly known as phase change material (PCM). Latent heat storage methods have caught a lot of attention recently due to their several attractive features like high energy storage density, isothermal operation properties, and economic feasibility [3,4]. Due to their massive potential, PCMs have been adopted in several engineering applications like heat sinks [5], solar energy storage [6], waste heat recovery [7], and building energy conservation [8].

The literature review shows different studies investigating the thermal performance of both organic and inorganic PCMs. Organic PCMs (paraffin, fatty acids) are thermochemically stable and thus considered more reliable for latent heat storage [9]. However, the performance of the organic PCMs in heat transfer applications is limited by low thermal conductivity which ranges between 0.1 and 0.3 W/mK. On the other hand, inorganic PCMs possess higher enthalpy, and thermal conductivity, and are considered a more economically viable option compared to organic PCMs. Some inorganic PCMs (salt hydrates) have shown short service lift due to their corrosive nature towards metals leading to a high system maintenance cost. This issue can be resolved by microencapsulation of the PCMs which can evade its leakage into the system [10,11].

Recent technological advancements have resulted in complex and compact systems and researchers around the world have invested significant efforts to improve their thermal management using different fin shapes and configurations [12–16] and nanofluids [17–22]. In addition, several efforts have been made to improve the thermal performance of the PCM-based heat transfer systems e.g., high conductivity particle dispersion [23], surface tension [24], and geometric design alteration

* Corresponding author at: Mechanical Engineering Department, Faculty of Engineering, P.O. Box 68151-44316, Lorestan University, Iran.
E-mail address: izadi.m@lu.ac.ir (M. Izadi).

https://doi.org/10.1016/j.icheatmasstransfer.2022.106421

Available online 14 October 2022

Nomenclature

w	*size of double thermal storage* (m)
x, y	dimensional *coordinates* (m)
X, Y	*dimensionless coordinates* (−)
AR	*aspect ration of fins* (−)
u, v	dimensional velocity components (ms^{-1})
U, V	dimensionless velocity components (ms^{-1})
F_o	*The* thermal Fourier number (−)
c	*porous zone constant*
f	*melted phase change material fraction*
t	*time* (s)
T	*temperature* (K)
p	*pressure* (Pa)
Pr	*Prandtl number* (−)
Nu	*Nusselt number* (−)
Ra	*Rayleigh number* (−)
A_{mushy}	*Mushy constant* ($kgm^{-3}\ s^{-1}$)
PCM	*phase change material*

Greek symbols

σ	*The melting fraction of PCM* (−)
α_R	thermal diffusivity ratio of the fin to PCM (−)
θ	*dimensionless temperature* (−)
λ_l, λ_r	angle of left-side and right-side fins, respectively (°)

Subscripts

Fin	*refer to fin*
p	*refer to phase change material*
f	*refer to initial temperature*
h	*refer to hot wall*

[25]. High thermal conductivity particles like metal nanoparticles [26,27], metal foams [28], and expanded graphite [29] are added to the PCM in the particle dispersion method. Hajizadeh et al. [30] investigated the thermal performance of nano-encapsulated PCM in a wavy channel heat exchanger for the solidification process. They used paraffin mixed with CuO nanopowders as nano-encapsulated PCM (NEPCM) and reported a 38% improvement in the process rate. Bouzennada et al. [16] performed thermal analysis on a rectangular capsule with and without the bisecting fin with variation of inclination angle using RT-27 as PCM. They reported that the melting time reduced with the inclination angle and utilizing a bisecting fin. Khedher et al. [27] conducted experimental and numerical analysis to study the performance of LHTES with combination of fins and NEPCMs and reduced the charging and discharging time by 62% and 71%, respectively. Shehzad et al. [31] performed numerical analysis on aqueous-based NEPCM in a heat exchanger with wing-like fins to study the impact of fin orientation on natural convection. They showed that the vertical alignment of fins leads to thermal performance augmentation. Wang et al. [32] conducted experiments to study the thermal performance of water with well-dispersed micro-encapsulated PCM (MEPCM) by varying the particle volume fractions. They reported a heat transfer enhancement of 1.34 times compared to pure water.

Fin integration is the most sought-after design alteration approach due to its simplicity and lesser cost penalty [33]. Joybari et al. [34] studied the impact of several geometric parameters on the charging and discharging processes. They concluded that different design configurations should be used for different heat storage systems. PCMs are also incorporated into several heat exchanger types [35–37]. Saeed et al. [36] performed experiments to determine heat exchanger thermal performance where water and hexadecane are used as the heat transfer fluid and PCM, respectively. They reported that the novel heat exchanger design shows good thermal performance with effectiveness values of 83%. Amagour et al. [37] investigated the compact finned-tube heat exchanger performance with Moroccan provenance PCM. They utilized the equivalent circular fin efficiency to compute the effective surface heat transfer area and claimed that the investigated heat exchanger configuration is well suited for solar-powered domestic heat pump systems. Medrano et al. [38] conducted an experimental analysis to investigate the performance of five commercial heat exchanger configurations employing water as the heat transfer fluid and paraffin RT35 as PCM. They reported that the highest average power is achieved with the double-coil heat exchanger using a graphite matrix and the highest average thermal power is measured with a finned-tube heat exchanger configuration. The analysis of a double spiral heat exchanger, shell side filled with paraffin/expanded graphite composite PCM was constructed by Zheng et al. [39]. Their numerical study led to the optimal radius ratios of 0.33 and 0.78 for the double spiral coil tubes. Shehzad et al. [40] performed numerical analysis to investigate Fe_3O_4 and multi-walled carbon nanotube hybrid nanoparticle flow under magnetic force. They claimed the working fluid tends to flow towards the souce of the magnetic force consequently impeding the flow. Hosseinzadeh et al. [41] utilized Galerkin Finite Element Method (GFEM) to numerically simulate the solidification process of water mixed with hybrid nanoparticles ($TiO_2 - Go$) as PCM in a triplex container with rectangular fins. They reported an acceleration of solidification process leading to a 12% shorter solidification time. Later, they studied ($MoS_2 - Fe_3O_4$) hybrid nanofluid in a star-shaped triplex latent heat thermal energy storage system and presented a 4% increment of solidification rate associated with hybrid nanofluid dispersion in the PCM [42]. In addition, they investigated the PCM solidification process and evaluated the sole/combined influence of fins and nanoparticles in a triplex-tube heat exchanger with rectangular fins in a tree-like arrangement using FlexPDE [43]. Other studies in literature analyzed PCM melting evolution [44], and hydro-thermal charcteristics of nanofluids in metal foam in different heat exchanger configurations [45,46].

Investigating heat transfer in non-square geometries have received much interest due to the complex heat transfer configurations that can be found in industrial applications. Among these geometries, the H-shaped one has been proven to have a better thermal performance than other geometries like the C-shape or T-shape [47]. The convective heat transfer of various fluids such as nanofluids in H-shaped enclosures has been considered [48]. As for the effect of fins in H-shaped cavities, it has been also studied in the case of pure fluids [49]. However, the case of PCM in an H-shaped finned enclosure has not yet been considered to the authors' knowledge. Due to the importance of the cavity shape, the presence of fins, and the PCM contribution, the present study is aimed at investigating the thermal performance of H-shaped thermal storage in a charging process with different fin configurations. Different design configurations of the H-shaped double thermal storage are modeled by varying the fin angle on both sides of the thermal storage in symmetric ($-60 \le \lambda \le 60$) and unsymmetric manner ($-60 \le \lambda_l \le 60; -60 \le \lambda_r \le 60$). Moreover, the fin aspect ratio is varied from 0.5 to 32 and the melting process of the PCM is investigated numerically. A comparative analysis is performed to achieve the optimal design configuration by comparing the thermal Fourier number for all the geometric configurations.

2. Physical model and governing equations

This study investigates the charging process of a double thermal storage unit filled with phase change material. A thermal storage unit like the one considered here can be used in solar panels as indicated in

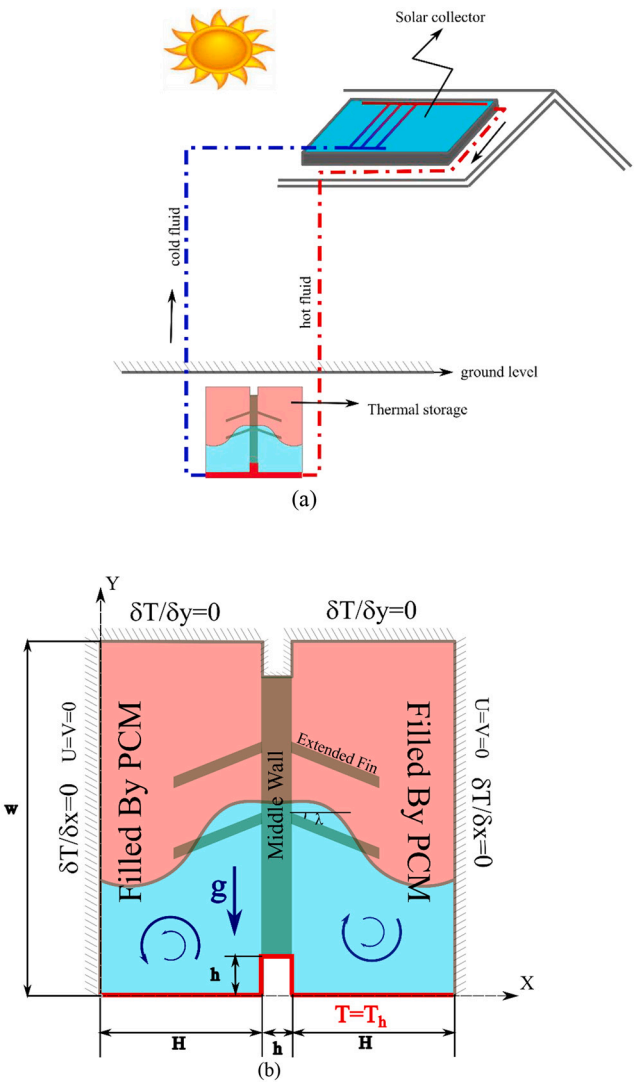

Fig. 1. Schematic view of the present problem (a) charging loop (b) thermal storage.

Fig. 1. which illustrates the schematic view of the present problem. It should be noted that the focus of the present study is on the finned PCM cavity as an innovative means of heat transfer and that some of the tested parameters might be in a range not applicable for solar panels. The double thermal storage unit is heated from the bottom wall while the other walls are kept adiabatic. Thermal energy can be absorbed from any renewable source such as solar collectors. The thermal storage is divided by a conducting finned wall into two separate parts which can intensify the charging process. The thermal energy which can be stored by the enclosure filled with Phase change material (PCM) plays the main role in energy management as the main part of any applied renewable energy source.

According to this figure, the heated wall has a fixed temperature, T_h, as thermal storage is charging.

The non-slip velocity is imposed on all walls. To incorporate the effects of buoyancy in the liquid phase of PCM, density is neglected as a variable in the momentum equation except for the buoyancy term. The Boussinesq approximation was used to model density variation in the buoyancy term.

Dimensionalized form of governing equations including continiuty, two dimentional momentum, and energy equations can be presented in the following form:

$$\frac{\partial u}{\partial x}+\frac{\partial v}{\partial y}=0 \tag{1}$$

$$\rho_p\left(\frac{\partial u}{\partial t}+\left(u\frac{\partial u}{\partial x}+v\frac{\partial u}{\partial y}\right)\right)=-\frac{\partial p}{\partial x}+\left(\frac{\partial}{\partial x}\left(\mu_p(1+c^{'}(1-f(T)))\frac{\partial u}{\partial x}\right)+\frac{\partial}{\partial y}\left(\mu_p(1+c^{'}(1-f(T)))\frac{\partial u}{\partial y}\right)\right)+N_x \tag{2}$$

$$\rho_p\left(\frac{\partial v}{\partial t}+\left(u\frac{\partial v}{\partial x}+v\frac{\partial v}{\partial y}\right)\right)=-\frac{\partial p}{\partial y}+\frac{\partial}{\partial x}\left(\mu_p(1+c^{'}(1-f(T)))\frac{\partial v}{\partial x}\right)+\frac{\partial}{\partial y}\left(\mu_p(1+c^{'}(1-f(T)))\frac{\partial v}{\partial y}\right)+N_y+\rho_p g\beta_p(T_h-T_s) \tag{3}$$

$$(\rho c_p)_p\frac{\partial T}{\partial t}+(\rho c_p)_p\left(u\frac{\partial T}{\partial x}+v\frac{\partial T}{\partial y}\right)+\left(\rho_p L_p\frac{\partial \gamma(T)}{\partial t}\right)=k_p\left(\frac{\partial^2 T}{\partial x^2}+\frac{\partial^2 T}{\partial y^2}\right) \tag{4}$$

Third terms at right hand side of the momentum equations are called the Carman- Kozeny which represent the momentum additional contribution due to the melting and freezing processes.

$$N_y=\omega(T)v, N_x=\omega(T)u, \omega(T)=-c^{'}\frac{(1-f(T))^2}{f(T)^3+\varepsilon} \tag{5}$$

The flowfield variables are converted to equivalent non-dimensionalized variables to rewrite the governing equations in non-dimensionalized form. The nondimensionalized variables are:

$$X=\frac{x}{w}, Y=\frac{y}{w}, V=\frac{vw}{\alpha}, U=\frac{uw}{\alpha}, P=\frac{pw^2}{\rho\alpha^2}, F_o=\frac{t\alpha}{w^2}, \zeta(\theta)=-A_{mushy}\frac{(1-\sigma(\theta))^2}{\sigma(\theta)^3+\varepsilon}, \theta=\frac{(T-T_f)}{(T_h-T_f)} \tag{6}$$

X and Y are the dimensionless coordinates in the x and y directions. V and U are Nondimensional velocity components in two directions. P and F_o are dimensionless pressure and time, respectively. The term of ζ is derived from the Carman- Kozeny equation, where σ is the liquid fraction, ε is a very low-value constant applied to prevent division by zero and A_{mushy} is a constant dependent on the morphology of the melting boundary [50]. Finally, θ is the dimensionless temperature. The melting fraction of the phase change material based on dimensionless temperature is defined as follows:

$$\sigma(\theta)=\begin{cases}0 & \theta<0\\ \dfrac{T-T_f}{T_h-T_f} & 0<\theta<\Delta\theta\\ 1 & \theta>\Delta\theta\end{cases} \tag{7}$$

$$\overline{\sigma}=\int_A \sigma(\theta)dA$$

Incorporating the above-mentioned nondimensionalized variables (6), the governing equations are stated in nondimensionalized form as [51]:

Momentum equation in the X direction:

$$\left(\frac{\partial U}{\partial F_o}+\left(U\frac{\partial U}{\partial X}+V\frac{\partial U}{\partial Y}\right)\right)=-\frac{\partial P}{\partial X}+Pr\left(\frac{\partial}{\partial X}\left((1+A_{mushy}(1-\sigma(\theta)))\frac{\partial U}{\partial X}\right)+\frac{\partial}{\partial Y}\left((1+A_{mushy}(1-\sigma(\theta)))\frac{\partial U}{\partial Y}\right)\right)+\zeta(\theta)U \tag{8}$$

Momentum equation in the Y direction:

$$\frac{\partial V}{\partial F_o}+\left(U\frac{\partial V}{\partial X}+V\frac{\partial V}{\partial Y}\right)=-\frac{\partial P}{\partial Y}$$
$$+Pr\left(\frac{\partial}{\partial X}\left(\left(1+A_{mushy}(1-\sigma(\theta))\right)\frac{\partial V}{\partial X}\right)+\frac{\partial}{\partial Y}\left(\left(1+A_{mushy}(1-\sigma(\theta))\right)\frac{\partial V}{\partial Y}\right)\right)+\zeta(\theta)V \quad (9)$$
$$+RaPr\theta$$

Energy balance equation for the PCM:

$$\frac{\partial\theta}{\partial F_0}+\left(U\frac{\partial\theta}{\partial X}+V\frac{\partial\theta}{\partial Y}\right)+\frac{1}{Ste}\left(\frac{\partial\sigma(\theta)}{\partial F_0}\right)=\left(\frac{\partial^2\theta}{\partial X^2}+\frac{\partial^2\theta}{\partial X^2}\right) \quad (10)$$

Energy balance equation for the solid domain:

$$\frac{\partial\theta}{\partial F_0}=\alpha_r\left(\frac{\partial^2\theta}{\partial X^2}+\frac{\partial^2\theta}{\partial Y^2}\right) \quad (11)$$

$$\alpha_R=\frac{\alpha_f}{\alpha_{PCM}}$$

Ra, Ste., *Pr*, α_R, *Pr* are the key parameters defined as Rayleigh number (ratio of buoyancy force to heat dissipation), Stefan number (Ratio of heat required to change the temperature to latent heat), thermal diffusivity ratio of the fin to PCM and Prandtl number.

The initial and boundary conditions corresponding to the non-dimensionalized governing equations have been represented in dimensionless form as follows:

Initial conditions:

$$\theta=0, U=V=0\forall F_0, X, Y\exists F_0=0$$

Boundary conditions on the bottom side:

$$\theta=1, U=V=0\forall F_0, X, Y\exists\begin{cases} Y=0, 0\le X\le 4.5\\ Y=0.1, 4.5\le X\le 5.5\\ Y=0, 5.5\le X\le 1\\ X=4.5, 0\le Y\le 0.1\\ X=5.5, 0\le Y\le 0.1\end{cases}$$

Boundary conditions on the upper side:

$$\frac{\partial\theta}{\partial Y}=0, U=V=0\forall F_0, X, Y\exists\begin{cases} Y=1, 0\le X\le 4.5\\ Y=0.9, 4.5\le X\le 5.5\\ Y=1, 5.5\le X\le 1\end{cases}$$

$$\frac{\partial\theta}{\partial X}=0, U=V=0\forall F_0, X, Y\exists\begin{cases} X=4.5, \mathrm{w}\le Y\le w-\mathrm{h}\\ X=5.5, 0.9\le Y\le 1\end{cases}$$

Boundary conditions on the left side:

$$\frac{\partial\theta}{\partial X}=0, U=V=0\forall F_0, X, Y\exists X=0, 0\le Y\le 1$$

Boundary conditions on the right side:

$$\frac{\partial\theta}{\partial X}=0, U=V=0\forall F_0, X, Y\exists X=1, 0\le Y\le 1 \quad (12)$$

The localized Nusselt number is estimated on the boundary of the hot wall using the expression stated below:

$$Nu_f=-\left(\frac{\partial\theta}{\partial n}\right)$$

$$Nu_{fin}=-\left(\frac{k_{fin}}{k_f}\right)\left(\frac{\partial\theta}{\partial n}\right) \quad (13)$$

Subscripts *f* and *fin* refer to the walls connected to PCM and fin, respectively. For the calculation of the averaged value, the localized Nusselt number is integrated over the hot bottom wall resulting in the

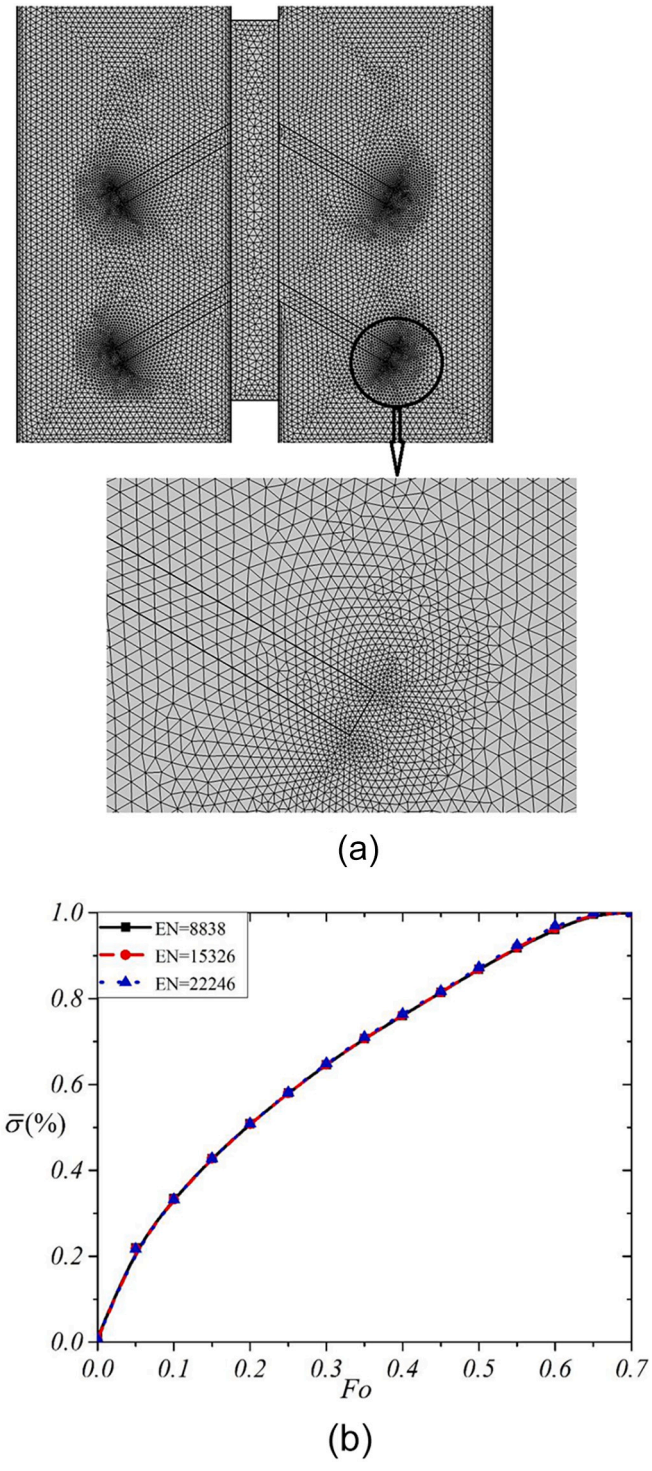

Fig. 2. (a) Sample of used grid (b) Grid size independence *Ra* = 1*e*6.

following expression:

$$Nu_{avg} = \frac{1}{w}\left(\int_{PCM\ area} Nu_f ds + \int_{fin\ area} Nu_{fin} ds\right) \quad (14)$$

3. Numerical method and validation

The flowfield of the computational problem can be reduced to partial, nonlinear differential equations which cannot be analytically resolved. Thus, the control volume-based finite element method (CVFEM) is incorporated to resolve the whole flowfield. Other methods include the finite difference method-a simple and relatively less accurate technique when dealing with irregular geometric configurations. On the contrary, finite element methods can deal with complex geometries and boundary conditions with significantly higher accuracy [52]. The computational domain is subdivided into smaller domains and the flowfield is solved using the solution of the differential equations at each element of the flowfield.

To ensure the computational results are independent of grid size, a grid independence study is performed. The grid size is systematically increased and the results are plotted in dimensionless parameters to conduct a comparative analysis. Fig. 2 shows that variation of the grid size does not have any significant effect on the results, thus a grid with a grid size of 8838 is used for all the simulations performed in the present study . For verification of the computational method, the computational results are compared to the published numerical data of *Al*-Jethelah et al. [53] who investigated PCM melting in a square enclosure with one heated wall while the three others are thermally insulated. The flow streamlines and isotherms shown in Fig. 3 demonstrate a good concordance between the two studies and, therefore, the verification of the numerical method.

In addition, the computational method is validated by comparison to the experimental results of Kamkari et al. [54] who measured melting progress of the PCM in a rectangular cavity. A comparison between the two results is presented in Fig. 4. under the same conditions. The striking similarity of the melting profile suggest that the computational results are fully consistent with the experimental data.

experimental data [54] (b) present work

Moreover, the experimentally [54] and numerically measured melting progress of the PCM in a rectangular cavity is presented in Fig. 4. under the same conditions. The striking similarity of the melting profile suggests the computational results are fully consistent with the experimental data.

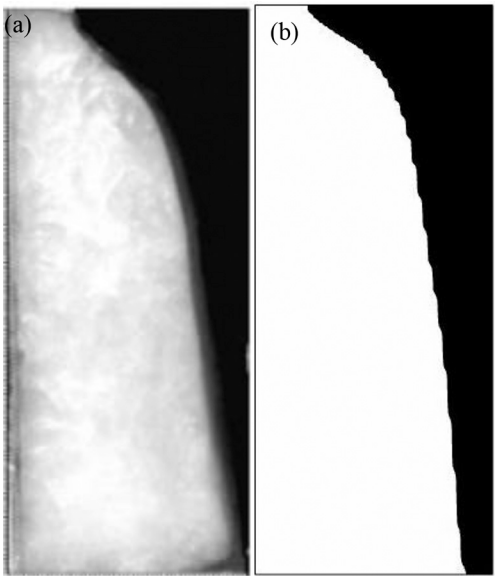

Fig. 4. The melting progress of PCM in the rectangular cavity with hot wall temperature (a)

4. Results and discussion

The effects of different key parameters, namely thermal Fourier number, fin angle (symmetric cases) ($-60 \le \alpha \le 60$), 15 cases related to non-symmetric fin angle ($-60 \le \alpha_l \le 60$ and $-60 \le \alpha_r \le 60$), and aspect ratio of fins (AR = 0.5–32) on the melting process of PCM are numerically analyzed. In this study, nondimensional parameters are considered at Pr = 28.32, Ra = 1e5, Ste. = 9e-2 and and $\alpha_R = 70$.

4.1. Effect of the thermal Fourier number and fin angle (symmetric cases)

Fig. 5 illustrates the evolution of isotherms and the velocity vectors with the thermal Fourier number *Fo* (i.e. the dimensionless time) for different values of the fin angle α. The presence of velocity vectors in a region inside the cavity indicates that the PCM is in the liquid phase in that region. In the early stage, for *Fo* = 0.1, the PCM starts to melt near the heated bottom wall. The heat is then rapidly transmitted from the bottom wall to the fins through the middle conductive wall. In the case without fins, the PCM melting first occurs near the bottom and middle walls, and then as the PCM keeps melting near the solid-liquid interface,

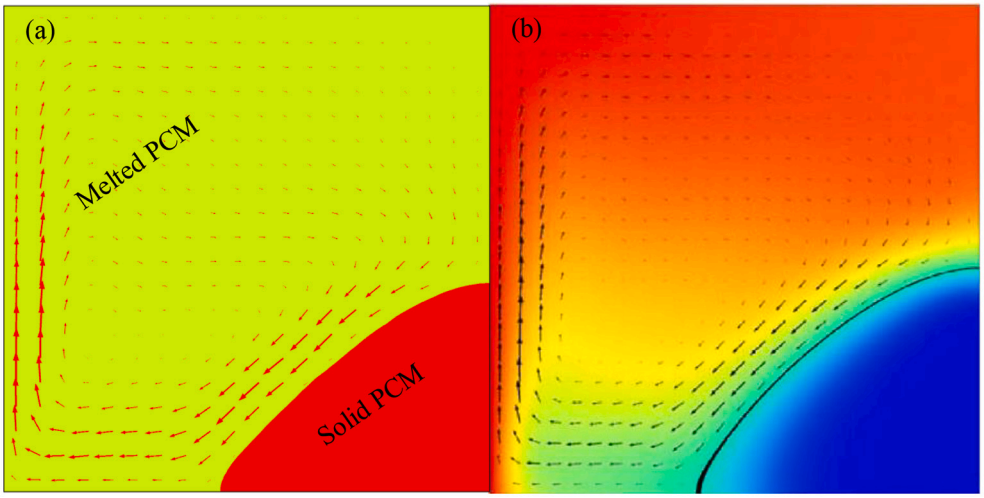

Fig. 3. Velocity vector and isothermal lines at *Ra* = 5e5, present work (left side) M. *Al*-Jethelah et al. [53] (right side)

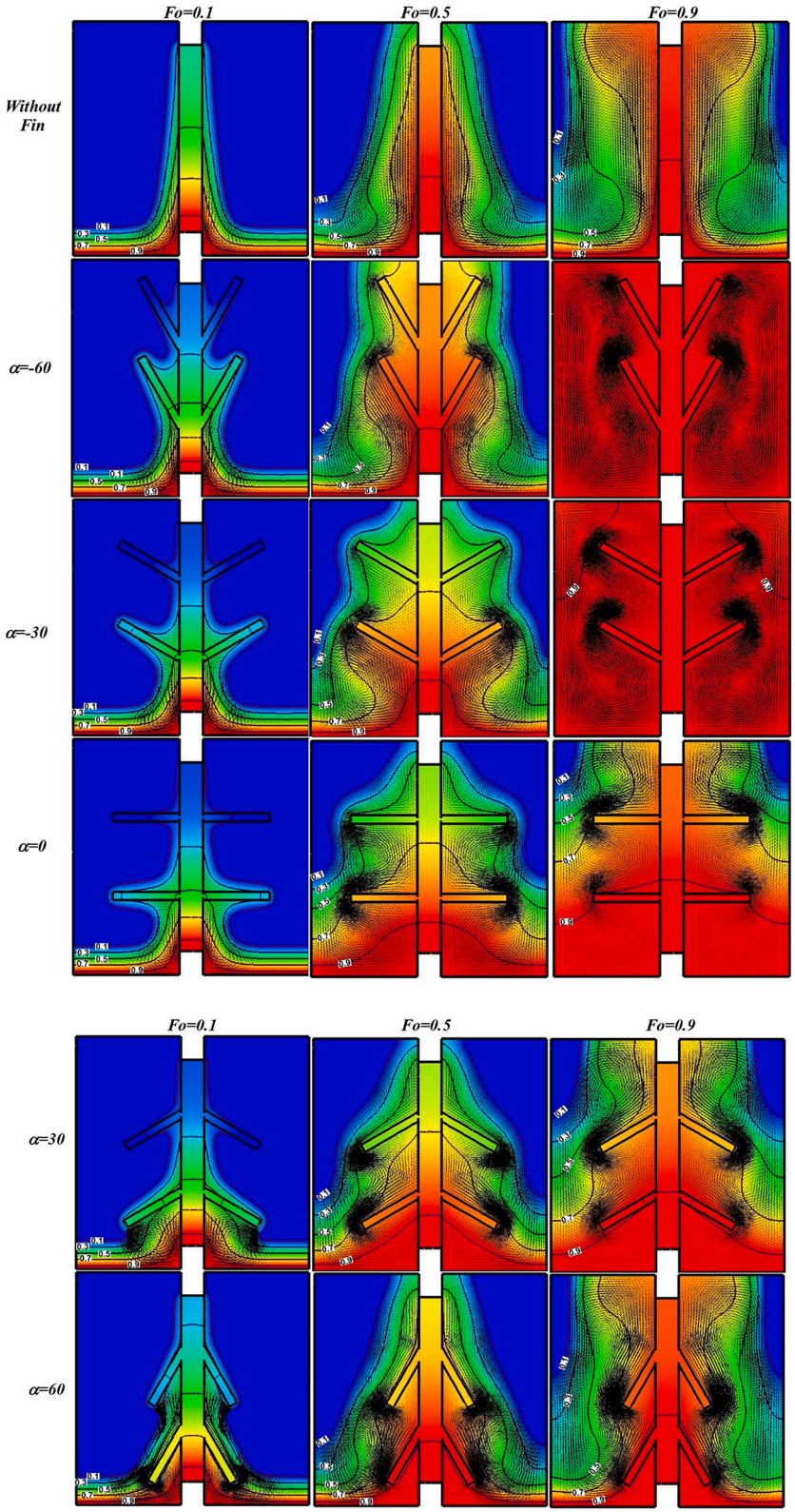

Fig. 5. Variation of isothermal lines and velocity vectors with respect to thermal Fourier number and fin angle (symmetric cases) at Ste. = 0.09, Ar = 8, Ra = 1e5

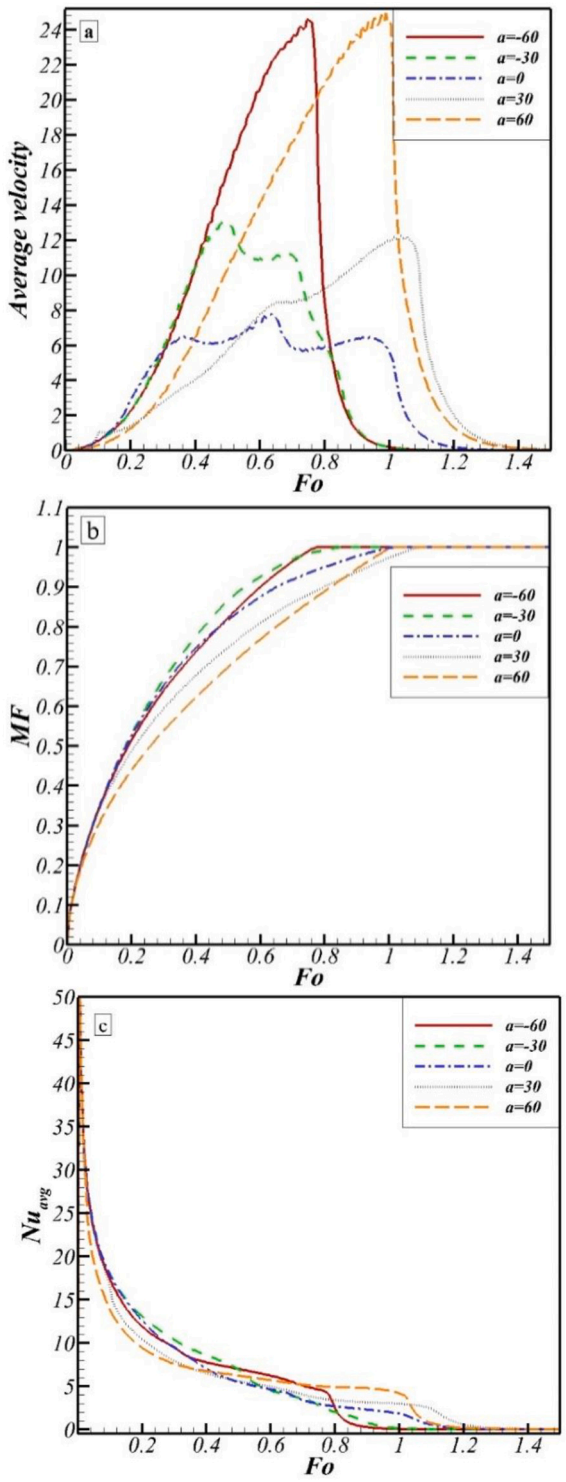

Fig. 6. Effect of fin angle (symmetric cases) versus The thermal Fourier number for (a) average velocity of Melted PCM, (b) melted fraction of PCM, and (c) averaged Nusselt number at Ste. = 0.09, Ar = 8, Ra = 1e5.

a convective flow takes place in the melted PCM as the hot liquid moves upwards and gets replaced by colder one incoming from near the melting interface. This results in two recirculation zones, one in the clockwise direction on the right side of the cavity, and the other in the counter-clockwise direction on the left side. The size of each zone keeps increasing as the PCM keeps melting. When fins are inserted, it can be seen that both the temperature and velocity fields are strongly perturbed near the fin edges. It is noted that a faster PCM melting is present for the

Table 1
Different combinations of non-asymmetric fin angles used in thermal storage

Case number	α_l	α_r	Case number	α_l	α_r
1#	0	−60	9#	−60	60
2#	0	−30	10#	−30	−30
3#	0	0	11#	−30	30
4#	0	30	12#	−30	60
5#	0	60	13#	30	30
6#	−60	−60	14#	30	60
7#	−60	−30	15#	60	60
8#	−60	30			

negative values of α, namely for $\alpha = -60^\circ$ and $\alpha = -30^\circ$, i.e. when the fins are inclined and directed upwards. Indeed, for negative values of α, the fins contribute to the PCM heating in the upper part of the enclosure. Without the fins, the PCM is mainly heated in the bottom and middle parts, then the thermal convection takes place. If the fins are directed downwards (positive α), the contribution of the fins is more in the bottom region, which doesn't affect significantly the PCM which is already being heated in that region. But when the fins are directed upwards, the PCM also is heated in the upper region which further contributes to PCM melting. Therefore, the main contribution of the fins is by transmitting heat to the PCM in the upper part of the cavity and accelerating PCM melting in addition to the already present convective effects. The variation of MF shows that, indeed, melting occurs faster for negative α values as discussed earlier.

The variations of the average velocity, the PCM melted fraction MF and the averaged Nusselt number Nu_{avg} as functions of *Fo* are plotted in Fig. 6. From the variation of the average velocity, two points can be noted. First, the maximum average velocity is achieved for $\alpha = 60^\circ$ and $\alpha = -60^\circ$ while the minimum is for $\alpha = 0$.

The presence of the fins obstructs fluid circulation. As the inclination of the fins increases, by decreasing the absolute value of α from 60° to 0, this obstruction becomes more important and the average velocity decreases to reach its minimum when the fins are horizontal for α=0. The fins have thus a double effect. In addition to transmitting heat to the PCM, they also slow down the flow circulation and inhibit the natural convention. This inhibition is intensified when the fins are horizontal. Using inclined fins can still transmit heat to the PCM while minimizing the flow obstruction. Second, the maximum is reached earlier in the case of negative α values compared to the positive ones. As for heat transfer, Nu_{avg} shows the same trend of variation for all the values of α.It starts with a high value when the PCM is still in the cold solid phase, then decreases substantially with PCM melting. As the PCM melting occurs faster when the fins are directed upwards, the intensity of the convective flow increases earlier compared to the other case. For this reason, also, it can be seen that Nu_{avg} is greater for negative α values throughout time and reaches a zero value faster in that case, as the thermal equilibrium is achieved earlier due to faster PCM melting.

4.2. Effect of the thermal Fourier number and fin angle (non-symmetric cases)

Table 1 presents the different cases of non-symmetric fin angles tested in the cavity. A parametric study is then conducted to analyze the thermal and flow behaviors of these cases.

The development of the streamlines in the cavity is depicted in Fig. 7 for the various cases of non-symmetric fins. It can be seen that the convective flow develops near the bottom wall and around the fins in all the cases. In the non-symmetrical configurations, in which the value of α is different between the left and right parts of the cavity, the flow patterns are also non-symmetrical around the middle wall. Moreover, the flow patterns in one part of the cavity are independent of the fin configuration in the other part. For instance, the flow behavior on the left side of the cavity is the same in cases 1 and 2, independently of the fin configuration on the right side.

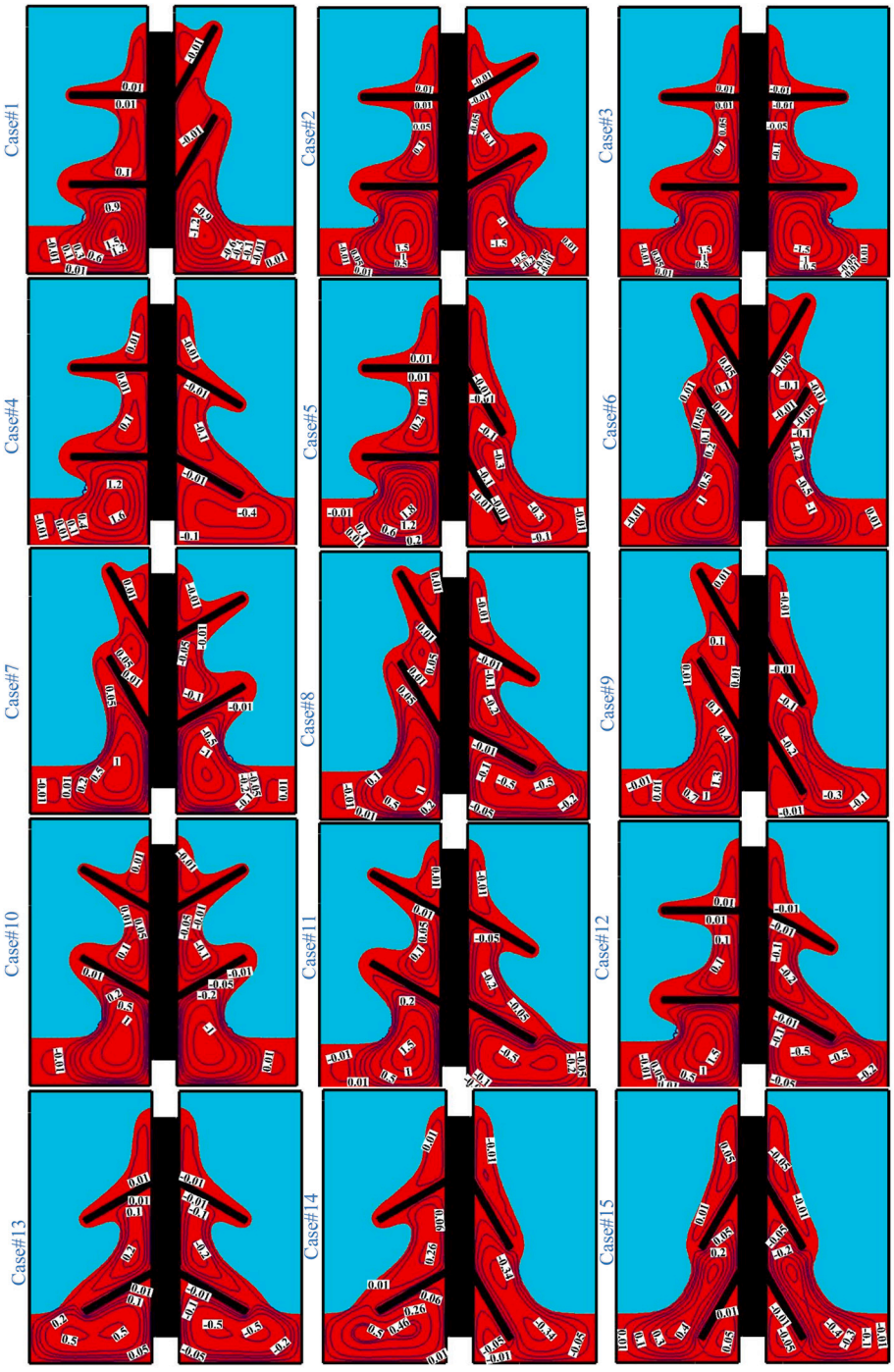

Fig. 7. Variation of streamlines in charged region (red color) respect to fin angle (non-symmetric cases) at Ste. = 0.09, Ar = 8, Ra = 1e5 (For interpretation of the references to color in this figure legend, the reader is referred to the web version of this article.)

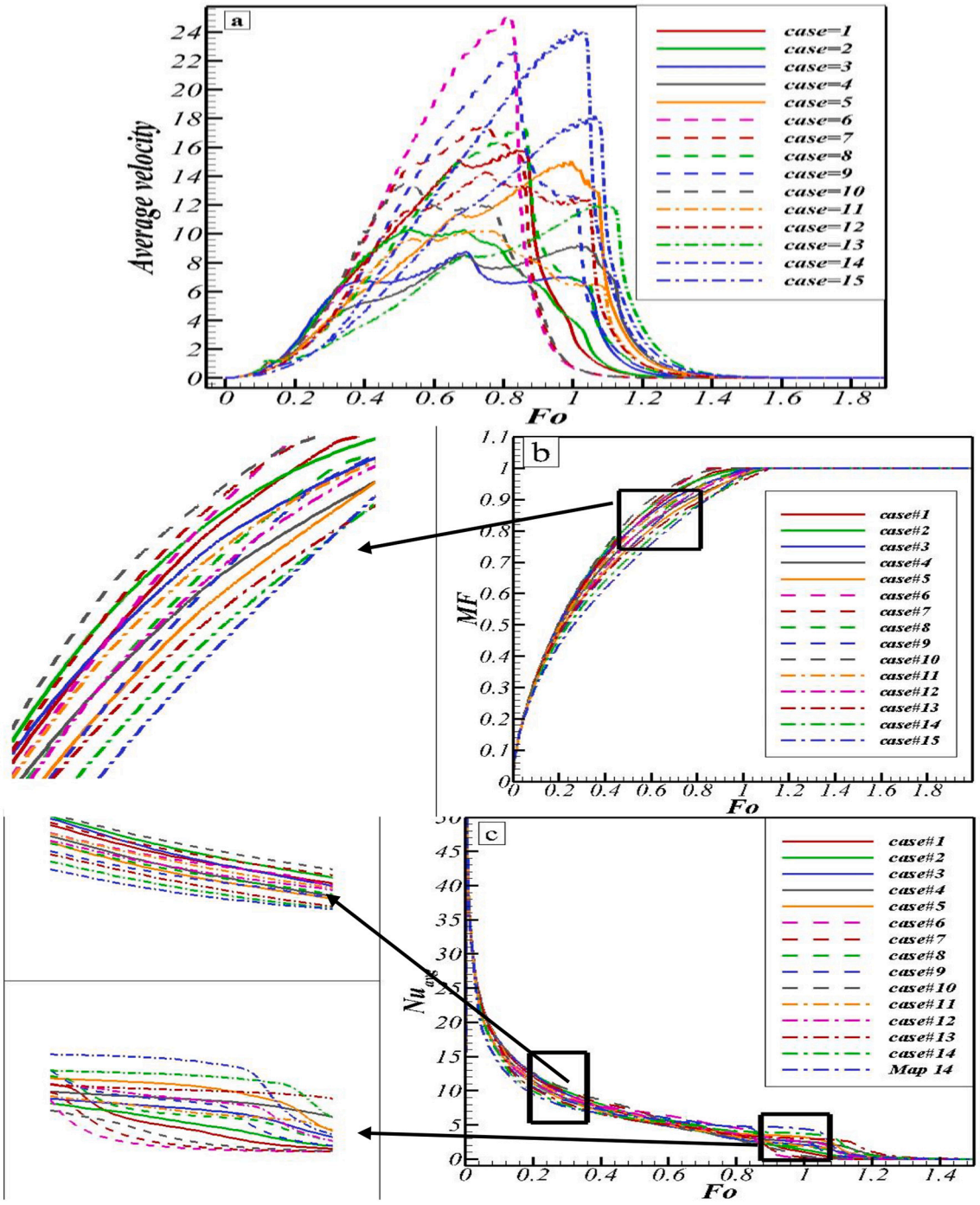

Fig. 8. Effect of fin angle (non-symmetric cases) versus The thermal Fourier number for (a) average velocity of Melted PCM, (b) melted fraction of PCM, (c) averaged Nusselt number at Ste. = 0.09, Ar = 8, Ra = 1e5

In general, the size of the recirculation zone occupies the whole bottom part of the enclosure for α higher than zero, due to the increased heat transfer in that region. However, when α is equal to or greater than zero, the flow is more developed in the middle and the upper cavity of the cavity, due to PCM undergoing more melting in that region compared to the cases in which $\alpha < 0$.

The effect of the fin angle on the variations of the average velocity, MF and Nu_{avg} as functions of *Fo* for the various non-symmetric cases are illustrated in Fig. 8.

The average velocity is maximum in case 6, for which $\alpha_l = \alpha_r = -60^\circ$, i.e. when the fins are directed upwards to the maximum extent. As PCM melting is undergoing at a fast rate at different locations in the cavity, the convective flow is intensified. The maximum is also reached in case 15, for $\alpha_l = \alpha_r = 30^\circ$, but at a later time compared to the case 6. Here, the fins also contribute to PCM heating at a fast rate while minimizing the flow obstruction, compared to the other cases. On the other hand, the average velocity is at its lowest in cases, like cases 3 and 4, where the fins are close to the horizontal due to the obstruction of flow

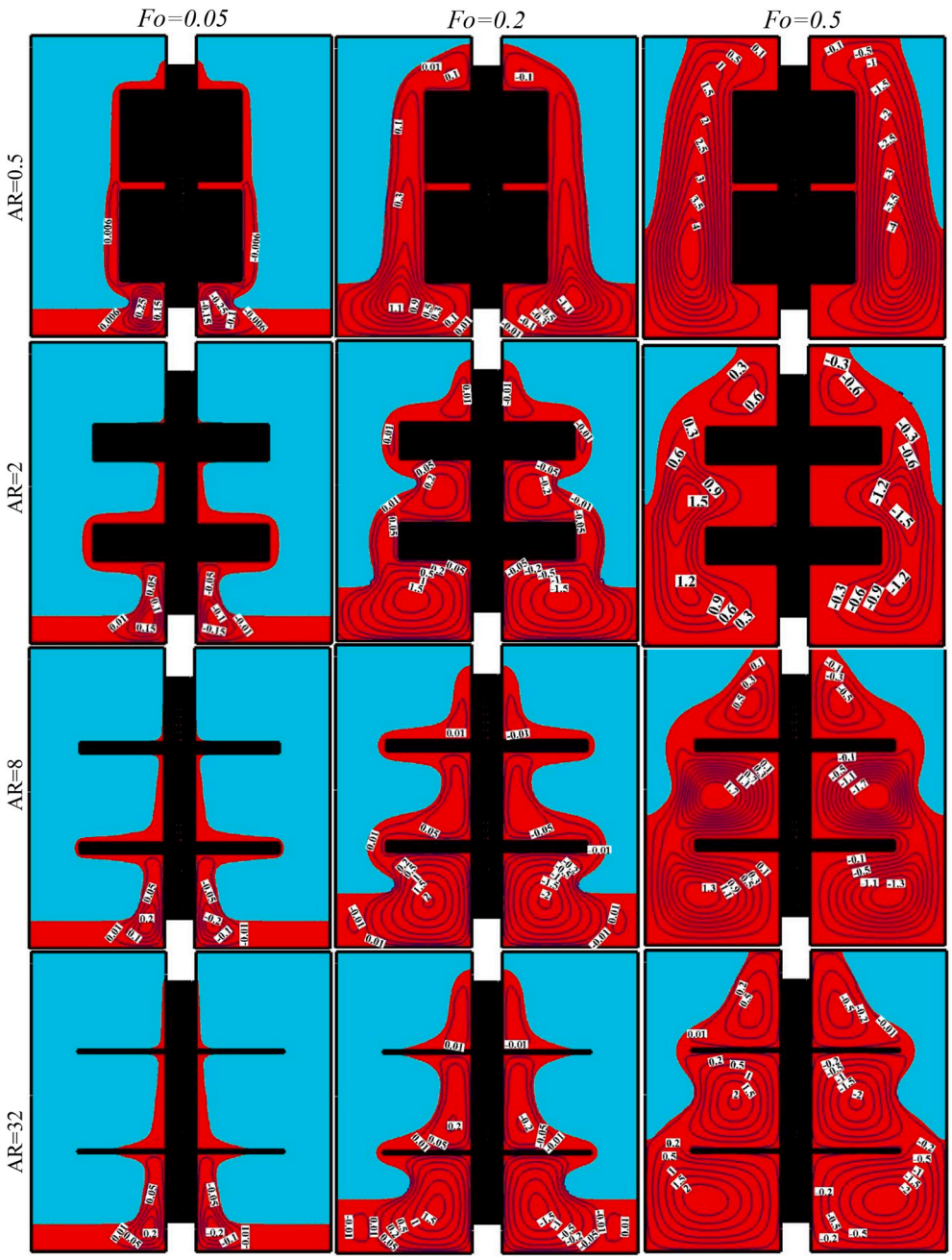

Fig. 9. Streamlines in melted PCM (red color) with respect to the thermal Fourier number and Aspect ratio of fins at Ste. = 0.09, *Ra* = 1e5

circulation. Following the intensity of the convective flow and heat transfer, the speed at which PCM melts is affected. A faster melting is achieved when the two fins are directed upwards, due to the PCM simultaneous heating in the top and bottom parts of the cavity. The variation of Nu_{avg} follows the speed at which the PCM is melting and is slightly higher when the fins are directed upwards in the cavity.

4.3. Effect of the thermal Fourier number and aspect ratio of fins

Aspect Ratio, Ar, is defined as the ratio of fin length to its thickness. Fig. 9 and Fig. 10 show the development of streamlines and the thermal distribution in the cavity for different values of the aspect ratio AR. Reducing AR increases the relative size of the fins and, consequently, decreases the allocated size of PCM in the cavity. In addition, it increases the surface of contact between the PCM and the fin, enhancing thus PCM melting. For AR = 0.5, one large recirculation zone appears in each part of the cavity. This is similar to a case in which a large conductive wall is situated in the middle of the cavity. As the fins don't restrict the fluid circulation, the convective flow covers all the height of the cavity and is intensified. As AR is increased above 0.5, several connected recirculation zones appear in each part delimited by two fins. In this case, the fins restrict the melt circulation. The intensity of the flow is diminished as a result, but increases as the fins get thinner when raising AR. For $AR = 0.5$, the isotherms are vertical in the whole cavity indicating a conduction-dominated heat transfer. When *AR* is increased, convection starts taking place near the bottom part of the cavity while conduction

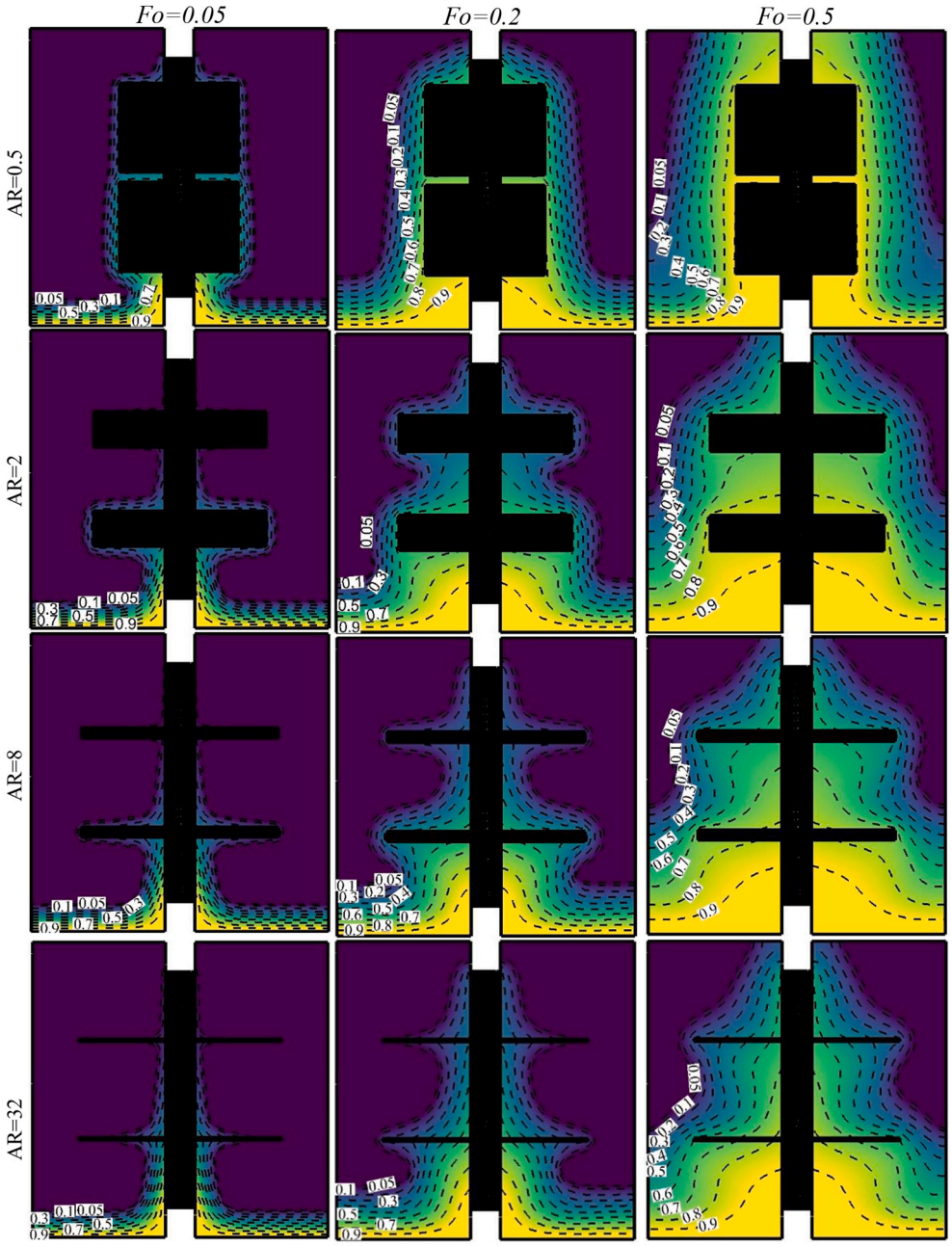

Fig. 10. Temperature distribution in melted PCM with respect to the thermal Fourier number and Aspect ratio of fins at Ste. = 0.09, *Ra* = 1e5

remains near the fins.

Fig. 11 shows the variations of the average velocity, MF and Nu_{avg} as functions of *Fo* for various values of AR. The average velocity is higher for AR = 0.5. The horizontal fins restrict the fluid circulation. When AR = 0.5, the fins length is substantially decreased to the point that the flow obstruction is limited which leads to high flow velocity. The intensification of the flow, in addition to the increase of the contact area between the PCM and the fins for lower AR, leads to a slower PCM melting when AR is raised.

5. Summary and conclusion

In the present study, the effect of using a fin inside an H-shaped cavity on the flow and thermal characteristics of a PCM during the charging process was investigated. In particular, the impact of the inclination angle of the fins, the non-symmetry in the cavity, and the aspect ratio of the fin were considered. The equations that govern the flow and heat transfer in the cavity were developed and converted into a non-dimensional form. The equations were solved using the Finite Element Method. The results were presented employing graphs of the streamlines and the isotherms, as well as in the variations with time of the average flow velocity, the melted fraction MF of the PCM, and the average Nusselt number Nu_{avg}. The main results can be summarized as follows:

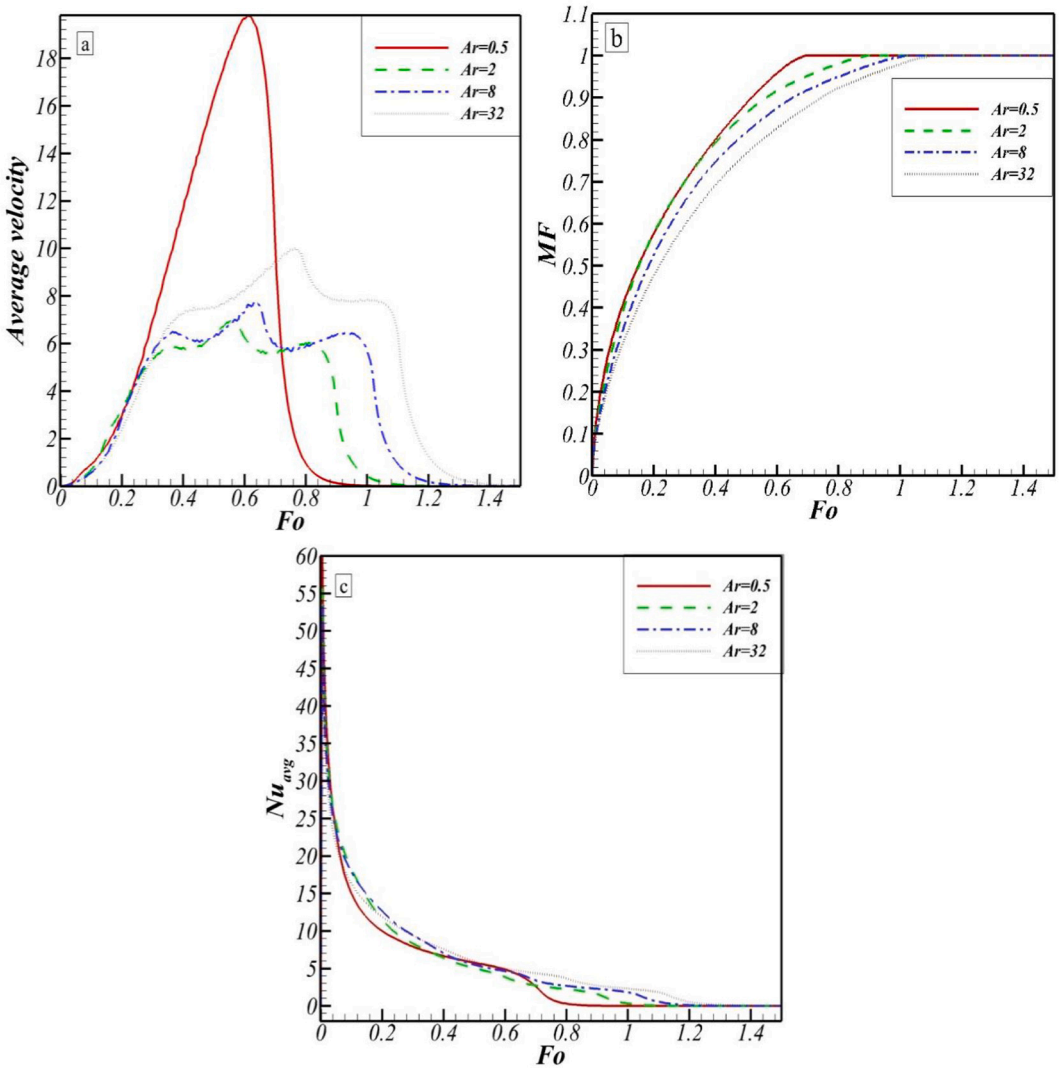

Fig. 11. Effect of the fin aspect ratio against thermal Fourier number for (a) average velocity of Melted PCM, (b) melted fraction of PCM, and (c) averaged Nusselt number

- ☞ Adding fins to the cavity enhances PCM melting in the neighboring region due to the conductive heat transfer through the fins.
- ☞ Directing the fins upwards contributes to heat transfer and PCM melting in the upper region of the cavity and intensifies the convective effect which results in faster PCM melting.
- ☞ Reducing the aspect ratio of the fins, for a fixed fin angle, enhances PCM melting due to increased contact between the fins and the PCM and a more uniform PCM heating throughout the cavity.

Declaration of Competing Interest

None.

Data availability

The authors do not have permission to share data.

References

[1] J. Pereira da Cunha, P. Eames, Thermal energy storage for low and medium temperature applications using phase change materials - a review, Appl. Energy 177 (2016) 227–238, https://doi.org/10.1016/j.apenergy.2016.05.097.

[2] S.A. Mohamed, F.A. Al-Sulaiman, N.I. Ibrahim, M.H. Zahir, A. Al-Ahmed, R. Saidur, B.S. Yılbaş, A.Z. Sahin, A review on current status and challenges of inorganic phase change materials for thermal energy storage systems, Renew. Sust. Energ. Rev. 70 (2017) 1072–1089, https://doi.org/10.1016/j.rser.2016.12.012.

[3] P.B. Salunkhe, P.S. Shembekar, A review on effect of phase change material encapsulation on the thermal performance of a system, Renew. Sust. Energ. Rev. 16 (2012) 5603–5616, https://doi.org/10.1016/j.rser.2012.05.037.

[4] K.H. Solangi, S.N. Kazi, M.R. Luhur, A. Badarudin, A. Amiri, R. Sadri, M.N. M. Zubir, S. Gharehkhani, K.H. Teng, A comprehensive review of thermo-physical properties and convective heat transfer to nanofluids, Energy. 89 (2015) 1065–1086, https://doi.org/10.1016/j.energy.2015.06.105.

[5] Z. Ling, Z. Zhang, G. Shi, X. Fang, L. Wang, X. Gao, Y. Fang, T. Xu, S. Wang, X. Liu, Review on thermal management systems using phase change materials for electronic components, Li-ion batteries and photovoltaic modules, Renew. Sust. Energ. Rev. 31 (2014) 427–438, https://doi.org/10.1016/j.rser.2013.12.017.

[6] A. Shukla, D. Buddhi, R.L. Sawhney, Solar water heaters with phase change material thermal energy storage medium: a review, Renew. Sust. Energ. Rev. 13 (2009) 2119–2125, https://doi.org/10.1016/j.rser.2009.01.024.

[7] L. Miró, J. Gasia, L.F. Cabeza, Thermal energy storage (TES) for industrial waste heat (IWH) recovery: a review, Appl. Energy 179 (2016) 284–301, https://doi.org/10.1016/j.apenergy.2016.06.147.

[8] F. Souayfane, F. Fardoun, P.H. Biwole, Phase change materials (PCM) for cooling applications in buildings: a review, Energy Build. 129 (2016) 396–431, https://doi.org/10.1016/j.enbuild.2016.04.006.

[9] M.M. Kenisarin, Thermophysical properties of some organic phase change materials for latent heat storage. A review, Sol. Energy 107 (2014) 553–575, https://doi.org/10.1016/j.solener.2014.05.001.

[10] W. Su, J. Darkwa, G. Kokogiannakis, Development of microencapsulated phase change material for solar thermal energy storage, Appl. Therm. Eng. 112 (2017) 1205–1212, https://doi.org/10.1016/j.applthermaleng.2016.11.009.
[11] W. Su, J. Darkwa, G. Kokogiannakis, Review of solid-liquid phase change materials and their encapsulation technologies, Renew. Sust. Energ. Rev. 48 (2015) 373–391, https://doi.org/10.1016/j.rser.2015.04.044.
[12] T. Ambreen, A. Saleem, H.M. Ali, S.A. Shehzad, C.W. Park, Performance analysis of hybrid nanofluid in a heat sink equipped with sharp and streamlined micro pin-fins, Powder Technol. 355 (2019) 552–563, https://doi.org/10.1016/j.powtec.2019.07.087.
[13] T. Ambreen, A. Saleem, C.W. Park, Numerical analysis of the heat transfer and fluid flow characteristics of a nanofluid-cooled micropin-fin heat sink using the Eulerian-Lagrangian approach, Powder Technol. 345 (2019) 509–520, https://doi.org/10.1016/j.powtec.2019.01.042.
[14] T. Ambreen, A. Saleem, C.W. Park, Pin-fin shape-dependent heat transfer and fluid flow characteristics of water- and nanofluid-cooled micropin-fin heat sinks: square, circular and triangular fin cross-sections, Appl. Therm. Eng. 158 (2019), https://doi.org/10.1016/j.applthermaleng.2019.113781.
[15] T. Ambreen, M.H. Kim, Effect of fin shape on the thermal performance of nanofluid-cooled micro pin-fin heat sinks, Int. J. Heat Mass Transf. 126 (2018) 245–256, https://doi.org/10.1016/j.ijheatmasstransfer.2018.05.164.
[16] T. Bouzennada, F. Mechighel, T. Ismail, L. Kolsi, K. Ghachem, Heat transfer and fluid flow in a PCM-filled enclosure: effect of inclination angle and mid-separation fin, Int. Commun. Heat Mass Transf. 124 (2021), 105280, https://doi.org/10.1016/j.icheatmasstransfer.2021.105280.
[17] T. Ambreen, M.-H. Kim, Comparative assessment of numerical models for nanofluids' laminar forced convection in micro and mini channels, Int. J. Heat Mass Transf. 115 (2017) 513–523, https://doi.org/10.1016/j.ijheatmasstransfer.2017.08.046.
[18] T. Ambreen, M.H. Kim, Effects of variable particle sizes on hydrothermal characteristics of nanofluids in a microchannel, Int. J. Heat Mass Transf. 120 (2018) 490–498, https://doi.org/10.1016/j.ijheatmasstransfer.2017.12.067.
[19] T. Ambreen, M.H. Kim, Heat transfer and pressure drop correlations of nanofluids: a state of art review, Renew. Sust. Energ. Rev. 91 (2018) 564–583, https://doi.org/10.1016/j.rser.2018.03.108.
[20] T. Ambreen, A. Saleem, C.W. Park, Thermal efficiency of eco-friendly MXene based nanofluid for performance enhancement of a pin-fin heat sink: experimental and numerical analyses, Int. J. Heat Mass Transf. 186 (2022), 122451, https://doi.org/10.1016/j.ijheatmasstransfer.2021.122451.
[21] T. Ambreen, A. Saleem, C.W. Park, Homogeneous and multiphase analysis of nanofluids containing nonspherical mwcnt and gnp nanoparticles considering the influence of interfacial layering, Nanomaterials. 11 (2021) 1–22, https://doi.org/10.3390/nano11020277.
[22] T. Ambreen, A. Saleem, M. Tanveer, K. Anirudh, A. Shehzad, C. Woo, Irreversibility and hydrothermal analysis of the MWCNTs / GNPs-based nanofluids for electronics cooling applications of the pin-fin heat sinks: multiphase Eulerian-Lagrangian modeling, Case Stud. Therm. Eng. 31 (2022), 101806, https://doi.org/10.1016/j.csite.2022.101806.
[23] J.M. Mahdi, E.C. Nsofor, Solidification enhancement of PCM in a triplex-tube thermal energy storage system with nanoparticles and fins, Appl. Energy 211 (2018) 975–986, https://doi.org/10.1016/j.apenergy.2017.11.082.
[24] Z. Khan, Z.A. Khan, Experimental investigations of charging/melting cycles of paraffin in a novel shell and tube with longitudinal fins based heat storage design solution for domestic and industrial applications, Appl. Energy 206 (2017) 1158–1168, https://doi.org/10.1016/j.apenergy.2017.10.043.
[25] W. Lin, Q. Wang, X. Fang, X. Gao, Z. Zhang, Experimental and numerical investigation on the novel latent heat exchanger with paraffin/expanded graphite composite, Appl. Therm. Eng. 144 (2018) 836–844, https://doi.org/10.1016/j.applthermaleng.2018.08.103.
[26] M.A. Kibria, M.R. Anisur, M.H. Mahfuz, R. Saidur, I.H.S.C. Metselaar, A review on thermophysical properties of nanoparticle dispersed phase change materials, Energy Convers. Manag. 95 (2015) 69–89, https://doi.org/10.1016/j.enconman.2015.02.028.
[27] N. Ben Khedher, R.A. Bantan, L. Kolsi, M. Omri, Performance investigation of a vertically configured LHTES via the combination of nano-enhanced PCM and fins: experimental and numerical approaches, Int. Commun. Heat Mass Transf. 137 (2022), 106246, https://doi.org/10.1016/j.icheatmasstransfer.2022.106246.
[28] X. Huang, Y. Lin, G. Alva, G. Fang, Thermal properties and thermal conductivity enhancement of composite phase change materials using myristyl alcohol/metal foam for solar thermal storage, Sol. Energy Mater. Sol. Cells 170 (2017) 68–76, https://doi.org/10.1016/j.solmat.2017.05.059.
[29] Z. Zhang, N. Zhang, J. Peng, X. Fang, X. Gao, Y. Fang, Preparation and thermal energy storage properties of paraffin/expanded graphite composite phase change material, Appl. Energy 91 (2012) 426–431, https://doi.org/10.1016/j.apenergy.2011.10.014.
[30] M.R. Hajizadeh, F. Selimefendigil, T. Muhammad, M. Ramzan, H. Babazadeh, Z. Li, Solidification of PCM with nano powders inside a heat exchanger, J. Mol. Liq. 306 (2020), https://doi.org/10.1016/j.molliq.2020.112892.
[31] S.A. Shehzad, B. Alshuraiaan, M.S. Kamel, M. Izadi, T. Ambreen, Influence of fin orientation on the natural convection of aqueous-based nano-encapsulated PCMs in a heat exchanger equipped with wing-like fins, Chem. Eng. Process. Process Intensif. 160 (2021), 108287, https://doi.org/10.1016/j.cep.2020.108287.
[32] Y. Wang, Z. Chen, X. Ling, An experimental study of the latent functionally thermal fluid with micro-encapsulated phase change material particles flowing in microchannels, Appl. Therm. Eng. 105 (2016) 209–216, https://doi.org/10.1016/j.applthermaleng.2016.05.159.
[33] M. Kazemi, M.J. Hosseini, A.A. Ranjbar, R. Bahrampoury, Improvement of longitudinal fins configuration in latent heat storage systems, Renew. Energy 116 (2018) 447–457, https://doi.org/10.1016/j.renene.2017.10.006.
[34] M.M. Joybari, F. Haghighat, S. Seddegh, A.A. Al-Abidi, Heat transfer enhancement of phase change materials by fins under simultaneous charging and discharging, Energy Convers. Manag. 152 (2017) 136–156, https://doi.org/10.1016/j.enconman.2017.09.018.
[35] W. Lin, R. Huang, X. Fang, Z. Zhang, Improvement of thermal performance of novel heat exchanger with latent heat storage, Int. J. Heat Mass Transf. 140 (2019) 877–885, https://doi.org/10.1016/j.ijheatmasstransfer.2019.06.040.
[36] R.M. Saeed, J.P. Schlegel, R. Sawafta, V. Kalra, Plate type heat exchanger for thermal energy storage and load shifting using phase change material, Energy Convers. Manag. 181 (2019) 120–132, https://doi.org/10.1016/j.enconman.2018.12.013.
[37] M.E.H. Amagour, A. Rachek, M. Bennajah, M. Ebn Touhami, Experimental investigation and comparative performance analysis of a compact finned-tube heat exchanger uniformly filled with a phase change material for thermal energy storage, Energy Convers. Manag. 165 (2018) 137–151, https://doi.org/10.1016/j.enconman.2018.03.041.
[38] M. Medrano, M.O. Yilmaz, M. Nogués, I. Martorell, J. Roca, L.F. Cabeza, Experimental evaluation of commercial heat exchangers for use as PCM thermal storage systems, Appl. Energy 86 (2009) 2047–2055, https://doi.org/10.1016/j.apenergy.2009.01.014.
[39] X. Zheng, N. Xie, C. Chen, X. Gao, Z. Huang, Z. Zhang, Numerical investigation on paraffin/expanded graphite composite phase change material based latent thermal energy storage system with double spiral coil tube, Appl. Therm. Eng. 137 (2018) 164–172, https://doi.org/10.1016/j.applthermaleng.2018.03.048.
[40] S.A. Shehzad, M. Sheikholeslami, T. Ambreen, A. Saleem, A. Shafee, Numerically simulated behavior of radiative Fe3O4 and multi-walled carbon nanotube hybrid nanoparticle flow in presence of Lorentz force, Appl. Math. Mech. 42 (2021) 347–356, https://doi.org/10.1007/s10483-021-2693-9. English Ed.
[41] K. Hosseinzadeh, A.R. Mogharrebi, A. Asadi, M. Paikar, D.D. Ganji, Effect of fin and hybrid nano-particles on solid process in hexagonal triplex Latent Heat Thermal Energy Storage System, J. Mol. Liq. 300 (2020), 112347, https://doi.org/10.1016/j.molliq.2019.112347.
[42] K. Hosseinzadeh, M.A.E. Moghaddam, A. Asadi, A.R. Mogharrebi, D.D. Ganji, Effect of internal fi ns along with hybrid nano-particles on solid process in star shape triplex latent heat thermal energy storage system by numerical simulation, Renew. Energy 154 (2020) 497–507, https://doi.org/10.1016/j.renene.2020.03.054.
[43] K. Hosseinzadeh, M.A.E. Moghaddam, A. Asadi, A.R. Mogharrebi, B. Jafari, M. R. Hasani, D.D. Ganji, Effect of two different fins (longitudinal-tree like) and hybrid nano-particles (MoS2-TiO2) on solidification process in triplex latent heat thermal energy storage system, Alexandria Eng. J. 60 (2021) 1967–1979, https://doi.org/10.1016/j.aej.2020.12.001.
[44] M.A.E. Moghaddam, M.R.H. Soukht, K. Hosseinzadeh, M. Behshad, D.D. Ganji, Metal foam and fin implementation into a triple concentric tube heat exchanger over melting evolution, Theor. Appl. Mech. Lett. 12 (2022), 100332, https://doi.org/10.1016/j.taml.2022.100332.
[45] T. Ambreen, A. Saleem, C.W. Park, Analysis of hydro-thermal and entropy generation characteristics of nanofluid in an aluminium foam heat sink by employing Darcy-Forchheimer-Brinkman model coupled with multiphase Eulerian model, Appl. Therm. Eng. 173 (2020), https://doi.org/10.1016/j.applthermaleng.2020.115231.
[46] T. Ur Rehman, T. Ambreen, H. Niyas, P. Kanti, H.M. Ali, C.W. Park, Experimental investigation on the performance of RT-44HC-nickel foam-based heat sinks for thermal management of electronic gadgets, Int. J. Heat Mass Transf. 188 (2022), 122591, https://doi.org/10.1016/j.ijheatmasstransfer.2022.122591.
[47] C. Biserni, L.A.O. Rocha, G. Stanescu, E. Lorenzini, Constructal H-shaped cavities according to Bejan's theory, Int. J. Heat Mass Transf. 50 (2007) 2132–2138, https://doi.org/10.1016/j.ijheatmasstransfer.2006.11.006.
[48] Z.A.S. Raizah, A.M. Aly, Natural convection in an H-shaped porous enclosure filled with a nanofluid, Comput. Mater. Contin. 66 (2021) 3233–3251, https://doi.org/10.32604/cmc.2021.012402.
[49] F. Keramat, A. Azari, H. Rahideh, M. Abbasi, A CFD parametric analysis of natural convection in an H-shaped cavity with two-sided inclined porous fins, J. Taiwan Inst. Chem. Eng. 114 (2020) 142–152, https://doi.org/10.1016/j.jtice.2020.09.011.
[50] V.R. Voller, C. Prakash, A fixed grid numerical modelling methodology for convection-diffusion mushy region phase-change problems, Int. J. Heat Mass Transf. 30 (1987) 1709–1719.
[51] S.M. Hashem Zadeh, S.A.M. Mehryan, M. Sheremet, M. Ghodrat, M. Ghalambaz, Thermo-hydrodynamic and entropy generation analysis of a dilute aqueous suspension enhanced with nano-encapsulated phase change material, Int. J. Mech. Sci. 178 (2020), 105609, https://doi.org/10.1016/j.ijmecsci.2020.105609.
[52] T.-R. Hsu, The Finite Element Method in Thermomechanics, Springer Science & Business Media, 2012.
[53] M. Al-Jethelah, S. Humaira Tasnim, S. Mahmud, A. Dutta, Melting of nano-PCM in an enclosed space: scale analysis and heatline tracking, Int. J. Heat Mass Transf. 119 (2018) 841–859, https://doi.org/10.1016/j.ijheatmasstransfer.2017.11.106.
[54] B. Kamkari, H. Shokouhmand, F. Bruno, Experimental investigation of the effect of inclination angle on convection-driven melting of phase change material in a rectangular enclosure, Int. J. Heat Mass Transf. 72 (2014) 186–200.